

MULTICOL-SLAM - A MODULAR REAL-TIME MULTI-CAMERA SLAM SYSTEM

S. Urban, S.Hinz

Institute of Photogrammetry and Remote Sensing, Karlsruhe Institute of Technology Karlsruhe
Englerstr. 7, 76131 Karlsruhe, Germany - (steffen.urban, stefan.hinz)@kit.edu
<http://www.ipf.kit.edu>

KEY WORDS: SLAM, multi-camera system, fisheye camera, bundle adjustment, egomotion estimation, loop closing

ABSTRACT:

The basis for most vision based applications like robotics, self-driving cars and potentially augmented and virtual reality is a robust, continuous estimation of the position and orientation of a camera system w.r.t the observed environment (scene). In recent years many vision based systems that perform simultaneous localization and mapping (SLAM) have been presented and released as open source. In this paper, we extend and improve upon a state-of-the-art SLAM to make it applicable to arbitrary, rigidly coupled multi-camera systems (MCS) using the MultiCol model. In addition, we include a performance evaluation on accurate ground truth and compare the robustness of the proposed method to a single camera version of the SLAM system. An open source implementation of the proposed multi-fisheye camera SLAM system can be found on-line <https://github.com/urbste/MultiCol-SLAM>.

1. INTRODUCTION

The accurate reconstruction of an observed scene from sets of ordered images has a long history in aerial (Kraus, 2004) and close-range photogrammetry (Luhmann et al., 2006). Usually, the object and reconstruction setup is well defined and the scene observations using high-resolution cameras are well planned. Thus, the connectivity between multiple camera positions is known or easily established and off-line bundle adjustment over the cameras and scene structure is performed yielding accurate results. In addition, initial values for the exterior and interior camera orientations are mostly available from external sensors, passpoints and accurate calibration.

In the computer vision community, the direction of research is called SfM and relaxes many constraints about scene and camera geometry that are assumed in classical photogrammetry. Advances in projective geometry (Hartley and Zisserman, 2008) and visual feature research (Weinmann, 2013) enabled the off-line reconstruction of large scenes from unordered sets of images and photo collections (Wu, 2013, Snavely et al., 2006, Agarwal et al., 2009, Wu et al., 2011, Szeliski, 2010, Sweeney et al., 2015b, Triggs et al., 2000). But essentially, the SfM methods solve the exact same problem as in aerial and (close-range) photogrammetry, i.e. reconstruction of scene and cameras. The main difference lies in the initialization of the bundle adjustment through direct relative orientation methods for calibrated (Stewenius et al., 2006, Hartley and Zisserman, 2008, Kneip et al., 2012) or uncalibrated (Barreto and Daniilidis, 2005, Kukulova et al., 2015) cameras and a simultaneous connectivity estimation using only natural image features.

In both communities, the scene is basically assumed to be static and the reconstruction is done off-line doing batch optimization over the entire scene. Hence, correspondence information (features) can be exhaustively extracted and matched a-priori and has no temporal coherence. Latter however, is the case for live video frames from a moving camera. In addition, the pose change (baseline and orientation) between subsequent frames can be very small.

Thus, the robotics community, where sensors (including cameras) are mounted on top of moving platforms, developed filter-based

methods (Davison et al., 2004, Montemerlo et al., 2002, Davison et al., 2007, Montemerlo and Thrun, 2007) to estimate the sensor pose from continuous sensor updates (live video). In recent years, basically two streams emerged from this line of research, namely filter- and keyframe-based SLAM techniques that will be described in more detail in the following. The basic idea behind both approaches is that not all poses, observations and uncertainties from a continuous video stream can (and have to) be integrated into the solution of the SLAM problem. Outstanding work of (Dellaert and Kaess, 2006) and (Strasdat et al., 2012) give a detailed analysis of both methods and close the gap between SLAM, SfM and classical bundle adjustment by generalization of the entire reconstruction problem using graphical models.

Figure 1 depicts the structure in an undirected graph (Markov Random Field) for a toy example. In total, four frames were recorded that observe a scene consisting of five map points. The poses are connected to map points by edges (observations) and the poses themselves are connected by state transitions (e.g. inertial sensor). An optimal BA solution is given (learned) by estimating the ML solution for the depicted graph and could be computed efficiently in this example. Speaking in terms of graphical models, the ML solution corresponds to the joint probability distribution over all parameters (poses and map points). Now, let's grow the graph by adding poses and map points. With each frame, the computational complexity increases and quickly exceeds the runtime constraints for real-time applications. Thus, we need a way of thinning out the graph. Using a filter-based approach, historic poses are marginalized out of the joint distribution by integration over all other parameters. The resulting graph is depicted in Figure 1b. The issue with filter-based SLAM becomes visible. To marginalize the current pose from the joint distribution, all potentials between connected variables need to be stored and updated with every frame and thus the number of map points will be very limited.

But especially a large map and many observed features lead to accurate and robust SLAM pipelines (Strasdat et al., 2012). Thus, the idea behind keyframe-based SLAM is to sparsify the graph by simply removing poses, map points and observations from the graph instead of marginalizing them from the probability distribution. In this way, classical BA can be performed which is efficient and fast to compute on sparse matrices (Triggs et al., 2000,

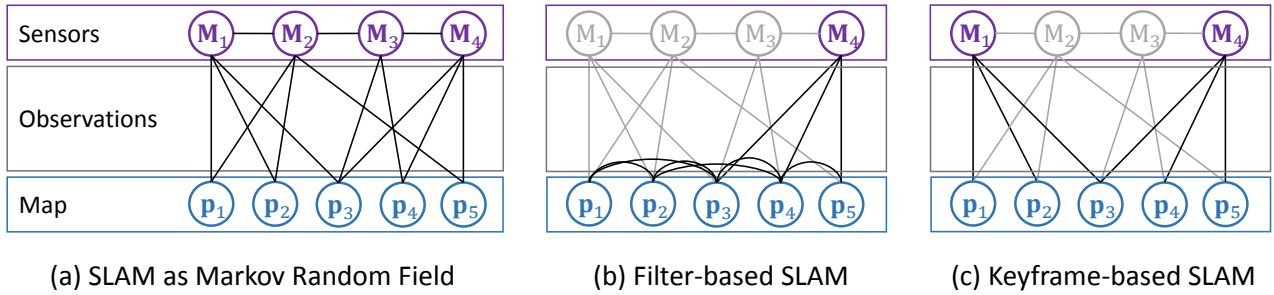


Figure 1. (a) SLAM as a Markov random field. (b) The graph is sparsified by marginalization of past poses except the current one from the graph. (c) Only keyframes are selected and all other poses, observations and object points, that are not visible in any retained keyframes are removed.

Kummerle et al., 2011)

Thus in this paper, a keyframe-based SLAM pipeline will be used as the basis for the continuous estimation of map and MCS pose. An additional benefit of using keyframes is, that the map points and observations that are connected to certain keyframes can be easily updated when the MCS revisits a place that changed.

In the following, we detail some related work. For a more detailed overview of available methods and features the reader is referred to (Garcia-Fidalgo and Ortiz, 2015, Gauglitz et al., 2011, Cadena et al., 2016).

2. STATE-OF-THE-ART

In recent years, plenty of keyframe-based SLAM systems were proposed and many of them are publicly available. Probably the first real-time SLAM system that was based on performing local and global BA over keyframes is PTAM, by Klein and Murray (Klein and Murray, 2007). One key to success was to split the tracking and mapping components of the system into separate threads running in parallel on a dual-core CPU. In this way, the mapping thread decides which camera poses to keep and store as keyframes and performs local and global BA asynchronously to the tracking thread. Latter runs at frame rate and performs matching of map point and camera pose estimation. Subsequently, PTAM was improved by adding edge features (Klein and Murray, 2008) and, with the increase in computing power, was implemented on a mobile phone (Klein and Murray, 2009). The use of image patches as features and the lack of loop closing mechanisms already suggests that large scale operation could be an issue using PTAM as storing, updating and indexing of image patches is costly. In addition, the global BA is performed over the entire scene, limiting its applicability to smaller workspaces.

To extend the range of PTAM, the authors of (Strasdat et al., 2010) propose a so-called scale-drift aware SLAM system. First, the keyframe decisions and feature initialization is moved to the tracking thread. Despite having a higher computational burden, the tracking becomes more stable, as features and keyframes are not initialized asynchronously and are immediately available for pose estimation. Due to the incremental nature of SLAM, the trajectory estimates start to drift over time, i.e. if the camera visits the same place twice, it will have a different exterior orientation and the reprojected map points exhibit large residuals to the measured image features. Still, if one is able to automatically detect similar places using place recognition methods (Garcia-Fidalgo and Ortiz, 2015), loop closing can be performed. The loop closing mechanism in (Strasdat et al., 2010) is based on SURF features and a dense surface model. Then, the trajectory is corrected

and optimized over similarity transformations, i.e. also correcting scale-drift.

Seminal work (Strasdat et al., 2011) focused on keyframe optimization, selection and constraints. Figure 2 depicts the double window approach. The inner window of active keyframes models the local area. Poses and map points are optimized using local BA. The outer window stabilizes the inner window and connects it to the rest of the trajectory. The question remains how to determine the connectivity between keyframes. In (Strasdat et al., 2011), the *co-visibility* is introduced. Instead of creating connections between keyframes based on geodesic or euclidean distance or temporal constraints, image features are used. By projecting map points to adjacent keyframes and matching their corresponding descriptors, a co-visibility weight can be calculated, that expresses how many equal features are visible in both keyframes. Apart from being able to update the connectivity if the scene changes, occlusions can be handled a lot better.

In (Pirker et al., 2011), a complete SLAM system was proposed including loop detection, re-localization and handling of long-term dynamics. Co-visibility and local map querying was not only constrained by image to image matches, but also on the level of map points. A Histogram of Cameras (HoC) descriptor (Pirker et al., 2010) is used to determine which map points are visible from the current camera pose. SIFT features are used and extraction and matching is performed on the GPU to achieve real-time performance, which limits its applicability on mobile platforms having only limited computing power.

In (Lim et al., 2014), the authors also build on the double-window optimization and co-visibility ideas but use the FAST detector coupled with BRIEF to exploit the performance of binary features. Using BRIEF and FAST decreases the time for feature extraction and matching significantly, however, this detector descriptor combination is not rotation and scale invariant and thus limited to in-plane trajectories (like driving cars). In addition, points are only queried and tracked from the last keyframe. Thus, the local map structure is not fully exploited. ORB-SLAM (Mur-Artal and Tardos, 2014, Mur-Artal et al., 2015, Mur-Artal and Tardos, 2016) is the latest state-of-the-art feature- and keyframe-based SLAM system, that is available on-line. As the name suggests, ORB features are used, being rotation and scale invariant to some degree. The map is reused and queried efficiently using co-visibility computed on ORB features. Place recognition is based on a binary BoW method (Gálvez-López and Tardós, 2012) and a new map initialization heuristic is introduced, that dynamically switches between fundamental and homography estimation. Robust keyframe and map-point culling heuristics ensure a high

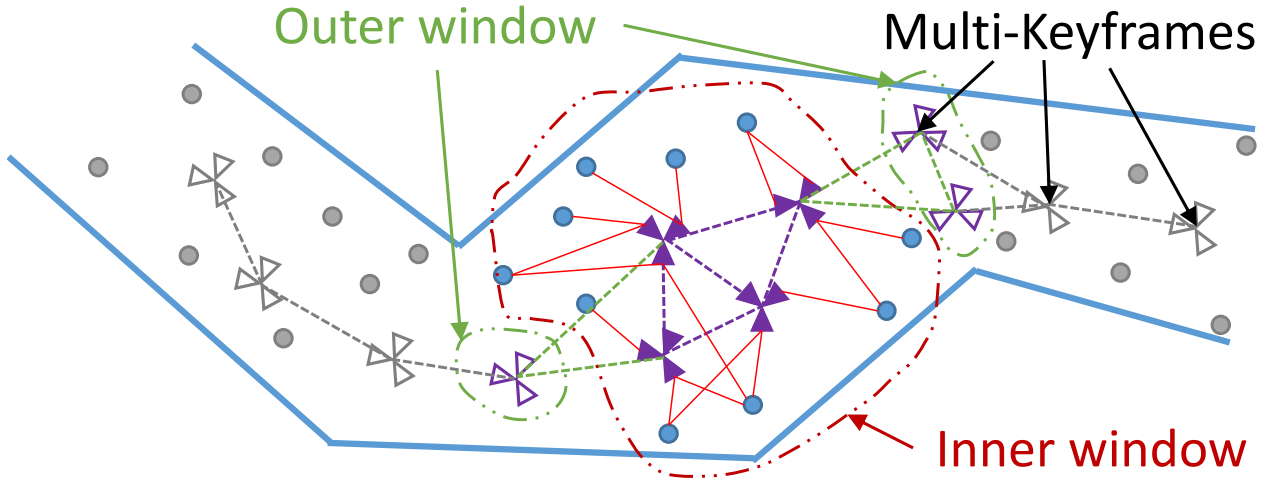


Figure 2. Principle of double window SLAM.

map quality. We will build our multi-fisheye camera SLAM upon ORB-SLAM and explain all changes in the next sections.

The methods described so far either use a single camera (Monocular SLAM) or a stereo configuration (Stereo SLAM). CoSLAM (Collaborative SLAM) (Zou and Tan, 2013) aims at combining the maps build by multiple cameras moving around in dynamic environments independently. The authors introduce inter-camera tracking and mapping and methods to distinguish static background points and dynamically moving foreground objects. In (Heng et al., 2014), four cameras are rigidly coupled on a MAV. Two cameras are paired in a stereo configuration respectively and self-calibrated to an IMU on-line. The mapping pipeline is similar to ORB-SLAM and also uses ORB descriptors for map point assignment. Additionally, the authors propose a novel 3-Point algorithm to estimate the relative motion of the MAV including IMU measurements. Most recent work on multi-camera SLAM is dubbed MC-PTAM (Multi-Camera PTAM) (Harmat et al., 2012, Harmat et al., 2015) and is build upon PTAM. In a first step (Harmat et al., 2012), the authors changed the perspective camera model to the generic polynomial model that is also used in this paper. This induces further changes, e.g. relating the epipolar correspondence search that now has to be performed on great circles on the unit sphere instead of point to line distances in the plane. In addition, significant changes concerning the tracking and mapping pipeline had to be made to include multiple rigidly coupled cameras. Keyframes are extended to MKFs as they now hold more than one camera. As PTAM, their system uses patches as image features and warps them prior to matching. Still, the system lacks a mapping pipeline that is capable to perform in large-scale environments. Subsequent work (Harmat et al., 2015) improved upon (Harmat et al., 2012) and is partly similar to the SLAM system developed in this thesis in that it uses the same camera model and g2o to perform graph optimization. On top, the authors integrated an automated calibration pipeline to estimate the relative orientation of each camera in the MCS. Still the system uses the relatively simple mapping back-end of PTAM instead of double-window optimization that is used in this thesis and has proven to be superior. In addition, image patches are used as features making place recognition, loop closing and the exploration and storage of large environments critical.

Thus far, all approaches were based on local point image features. Hence, the reconstructed environment will stay relatively sparse even if hundreds of features are extracted in each keyframe. This makes it difficult for autonomous vehicles or robots that explore

their surrounding to automatically analyze and extract object structure or texture information. Thus, most of the time, camera localization is coupled with laser scanners (Lin et al., 2012), structured light (Kerl et al., 2013), yielding structured object information. Recent work on semi-dense (Forster et al., 2014, Engel et al., 2014) and dense (Newcombe et al., 2011, Concha and Civera, 2015) camera-based SLAM systems make use of a single camera to estimate dense scene structure instead of reconstructing only point features.

LSD-SLAM (Engel et al., 2014) is a semi-dense approach that runs on a single CPU in real-time, in contrast to dense methods (Newcombe et al., 2011) that need heavy GPU support. Using direct image-alignment by minimizing the photometric error between image discontinuities, the method skips the costly feature extraction and matching stage of all feature-based SLAM systems. The time saved compensates for the increased BA runtime, as a huge number of observations is included. In addition, all scale-drift aware loop closing and large scale double window optimizations are included, making LSD-SLAM a state-of-the-art approach that also runs in real-time. However, loop closing uses FAB-MAP (Cummins and Newman, 2010) for place recognition and thus requires SURF features to be extracted. Subsequent work extended the method to mobile phones (Schöps et al., 2014), stereo (Engel et al., 2015) as well as omnidirectional cameras (Caruso et al., 2015). Instead of coupling camera pose estimation and semi-dense mapping, in (Mur-Artal and Tardós, 2015) a semi-dense extension to ORB-SLAM is presented. The semi-dense map is reconstructed from feature-based keyframes using depth consistency tests and a novel correspondence search. The semi-dense reconstruction is not obtained in real-time but is calculated in a CPU thread running in parallel to tracking and mapping. The methods yields superior performance compared to LSD-SLAM and it seems that the decoupling is advantageous, especially in dynamic scenes.

3. CONTRIBUTIONS

We will extend the state-of-the-art ORB-SLAM to multi-fisheye camera systems using MultiCol (Urban et al., 2016b). Our contributions to ORB-SLAM (and ORB-SLAM2 respectively) are the following:

1. The introduction of Multi-Keyframes (MKFs).

2. A hyper-graph formulation of MultiCol.
3. Multi-Camera loop closing.
4. Minimal non-central absolute pose estimation methods for re-localization (Kneip et al., 2013).
5. Different initialization method, based on the essential matrix.
6. Several performance improvements.

In order to use MultiCol, the concept of Multi-Keyframes (MKFs) is introduced. Employing a generic camera model (Scaramuzza et al., 2006) allows to couple arbitrary central cameras to the MCS. Instead of employing image patches as features (cf. MC-PTAM), compact binary descriptors proved to be the state-of-the-art when it comes to efficient large-scale re-localization, tracking and loop closing.

4. FRAMEWORK

In this chapter, the proposed SLAM system is introduced. As mentioned previously, the basic structure of our system is build upon ORB-SLAM (Mur-Artal and Tardos, 2014, Mur-Artal and Tardos, 2016). The proposed tracking and mapping system is dubbed MultiCol-SLAM. Figure 5 depicts an overview of the system. In general it is divided into multiple threads running in parallel and taking care of different aspects. For the sake of clarity, the loop detection thread is omitted in this figure. Each adaption to the original ORB-SLAM system is highlighted in red and will be explained in more detail in the following. Two of the most profound adjustments in MultiCol-SLAM compared to ORB-SLAM are the introduction of Multi-Keyframes (MKFs), i.e. a keyframe consists of multiple images and the use of fisheye cameras. Both novelties involve some significant changes to the basic design, e.g. bundle adjustment, pose estimation, map point triangulation and relative orientation computation.

With every new set of incoming camera images, the tracking thread extracts point features from every image. Then, they are stored in a continuous vector, that will later be used to identify and match points across MKFs and mask outliers. To ensure a fast indexing and querying of feature to camera mappings, we use hash maps (unordered maps in C++) that provide constant time $O(1)$ search. Like ORB-SLAM, we use the relative orientation between the last two frames to predict the current position of the system. The local map points are projected to the MCS and matched to the extracted features from the current frame. If enough matches are retained from the set of putative correspondences after an initial robust pose optimization using MultiCol, the tracking thread starts to search for more matches, assigns the reference MKF and decides if a new MKF should be added and passed over to the mapping thread. If the initial pose estimation fails, GP3P (Kneip et al., 2013) and RANSAC are used to perform re-localization of the MKS using the map points assigned to a set of recent MKFs. This is different compared to ORB-SLAM where a single camera and the non-minimal PnP solver EPnP (Lepetit et al., 2009) is used in a RANSAC loop to find potential map point matches and estimate the current camera pose after tracking failure. The tracking thread is detailed in Section 4.3.

Each time the tracking thread passes a new MKF to the mapping thread, recently created map points that do not fulfill certain conditions are deleted from the map. Then, new map points are triangulated over MKFs that are in the vicinity of the added MKF.

Here, the vicinity is determined by the co-visibility graph. In contrast to ORB-SLAM, where features are only triangulated between images of the same camera, the reconstruction is now performed over images of different cameras as well. Subsequently, local bundle adjustment is performed to adjust the poses of the MKFs that are part of the local map, as well as all map points. In addition, the mapping thread decides which MKFs are redundant and deletes them from the map. The mapping thread is detailed in Section 4.4.

The loop closing thread searches for potential loop closures with every new MKF that is added. To decide if a place was already visited before and to identify MKFs as loop candidates, the system uses a Bag-of-Binary-Words framework (Gálvez-López and Tardós, 2012). If a loop is detected, the essential graph (a sparse version of the co-visibility graph) is optimized. To correct for the scale-drift, the optimization is carried out over similarity transformations that connect the MKFs.

Like ORB-SLAM, we use the graph optimization framework g2o (Kummerle et al., 2011) for all optimizations. The difference to ORB-SLAM is how we model the tracking and mapping pipeline. As multiple cameras observe the scene from each pose (Figure 1) and also one map point can be observed by multiple cameras at the same time, the graph can not be represented by binary edges anymore (edges that connect two vertexes). Instead, we extend the graph to a hyper graph that we used to model MultiCol (cf. Figure 4) where edges can connect to an arbitrary number of vertexes.

4.1 The MultiCol Model

In this short subsection, we will briefly recapitulate the MultiCol model. For a more in-depth introduction to MultiCol and the involved camera model the reader is referred to (Urban et al., 2015, Urban et al., 2016b).

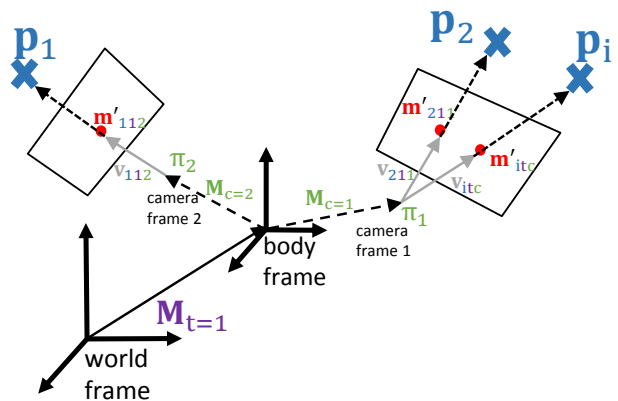


Figure 3. Depicted is the body frame concept and all involved parameters.

Given a homogeneous transformation matrix \mathbf{M} the transformation and projection of a world point \mathbf{p}_i to its corresponding image point \mathbf{m}_{itc} in camera c at time t is given by:

$$\mathbf{m}_{itc} = \pi_c^g(\mathbf{p}_{itc}) = \pi_c^g(\mathbf{M}_c^{-1}\mathbf{M}_t^{-1}\mathbf{p}_i) \quad (1)$$

where π_c^g is the generic camera model presented in (Scaramuzza et al., 2006, Urban et al., 2015) modeling all types of central cameras. If only perspective cameras are used, this could be exchanged with the calibration matrix \mathbf{K} and some additional distortion coefficients.

In the next section, the basic entities and methods that are used to represent the environment, i.e. map points, Multi-Keyframes and the co-visibility graph are detailed.

4.2 Map Entities

Map Points The map point is the most basic entity of the framework. Each map point \mathbf{p}_i has the following attributes, properties and variables:

- The 3D position $\mathbf{p}_i = [X_i, Y_i, Z_i]^T$ in world coordinates.
- A maximum d_{max} and minimum d_{min} distance at which the point can be observed. This distance is used to reduce the number of points that are queried for local map tracking.
- The viewing direction $\mathbf{n}_i = [n_x, n_y, n_z]^T$.

Multi-Keyframes In contrast to ORB-SLAM, each keyframe stores multiple images and is thus called Multi-Keyframe. Again, each Multi-Keyframe MKF_t created at time t has a number of attributes and variables:

- The MCS pose \mathbf{M}_t .
- A MCS object that stores the intrinsics of each involved camera and the extrinsics (\mathbf{M}_c) of the MCS. This object also performs the forward and back projection of world and image points.
- All features that are extracted from each camera. The features are stored in continuous vectors and thus a fast feature to camera search is needed. For each image point, we store two representations. One is its 2D image coordinate \mathbf{m}' that we use extensively in MultiCol bundle adjustment and pose estimation. In addition, we store the corresponding 3D bearing vector \mathbf{v} . Latter will be used in various geometry related algorithms, e.g. essential matrix estimation, epipolar search and absolute pose estimation (GP3P).
- The Bag-of-Binary-Words representation.

Co-Visibility Graph As in ORB-SLAM, the co-visibility graph is represented as a weighted undirected acyclic graph. The weight χ of each edge that connects two nodes (MKFs) in the graph is calculated as the number of map points the two MKFs share. In (Strasdat et al., 2011), a minimum weight χ_{min} between 15 and 30 was used to insert a connection. In contrast, the authors of ORB-SLAM do not impose a constraint on the minimal weight. When needed, the co-visibility graph is queried with a threshold, to only return nodes with a weight larger than χ_{min} , but the connectivity is kept very dense.

Map Initialization The initialization of the system comprises the estimation of an initial map and the corresponding camera poses. In general, the initialization of the map is the first crucial step in camera based SLAM system. The accuracy and robustness of the initial reconstruction has a significant impact on the overall performance of the system.

The authors of ORB-SLAM introduce an algorithm that switches between scene reconstruction using the fundamental matrix \mathbf{F} or estimating a homography \mathbf{H} using a heuristic. In general, this is a challenging task and often ignored, assuming the first camera motion introduces enough parallax. If a homography describes

the current scene better, i.e. if the camera is only rotating or observes a completely planar scene, initialization is suppressed. If a proper fundamental matrix is found, the scene is initialized, by reconstructing camera poses and scene points, followed by bundle adjustment eliminating the gauge freedom by fixing the first camera.

With MultiCol-SLAM, two issues arise that require some adaption. On the one hand, both \mathbf{F} and \mathbf{H} matrices contain the perspective camera matrix \mathbf{K} . For omnidirectional or fisheye cameras and especially the camera model employed in this work, a camera matrix does not exist. Still, if images points would be undistorted to their corresponding location in a perspective image, an application would be possible, although points at the image border would be lost. On the other hand, we are actually looking for the relative motion between two MCSs. Thus a map has to be initialized for each camera separately and then fused somehow. A different approach is to directly estimate the relative orientation between two MCS poses which is equivalent to computing the relative pose between two generalized cameras (Yu and McMillan, 2004). We experimented with the linear 17-pt (Yu and McMillan, 2004), a 6-pt (Stewenius et al., 2005) and a 8-pt algorithm (Kneip and Li, 2014) all part of OpenGV. The two polynomial solvers are relatively slow and the linear 17-pt algorithms is numerically very unstable. Recently, a new method was published (Ventura et al., 2015) but we leave the investigation for future work.

As the initial reconstruction of the SLAM trajectory is not at the core of this work, we propose a rather practical than generic methodology. We estimate an essential matrix \mathbf{E} in a RANSAC loop between the same camera from different MCS poses and choose the one with the most inliers and the highest translational magnitude. Then, we exploit a slight overlap between the FoVs and search for the map point projection in all other cameras. Finally, we perform bundle adjustment over all observations and the two MCS poses. This routine, however, only works robustly if small overlap exists.

4.3 Tracking Thread

In this section, the tracking thread is detailed. It is the core of our multi-camera tracking system as it handles not only the current state but performs feature extraction, matching and pose estimation. At the same time, it is the only thread that has to run in real-time, i.e. at frame rate. If this is not the case, incoming camera images will be dropped and tracking will suffer. Thus, an efficient implementation of all methods is essential. In addition, the tracking thread handles the MKF insertion and takes care of distributing work to all other threads.

All optimizations are carried out using iterative re-weighted least squares (IRLS) using Levenberg-Marquardt regularization and a robust Huber kernel. Huber suggested to calculate the tuning constant e as $e = 1.345\sigma$, where σ is some estimate of the standard deviation of the residuals, that we set to $\sigma = 2$. After each optimization, outlier edges (measurements) are found and eliminated by testing the residual against the Huber value.

Feature extraction The standard ORB detector extracts FAST corners at multiple scale levels (usually 8) and retains a certain number of corners per level that fulfill the Harris cornerness measure. In ORB-SLAM each image is additionally divided into several cells on each pyramid level. Then, the extractor tries to find at least 5 corners per cell to ensure a homogeneous distribution of feature points in the image. If this is not the case the cornerness threshold is adapted. Finally, the feature orientation and a ORB descriptor is computed.

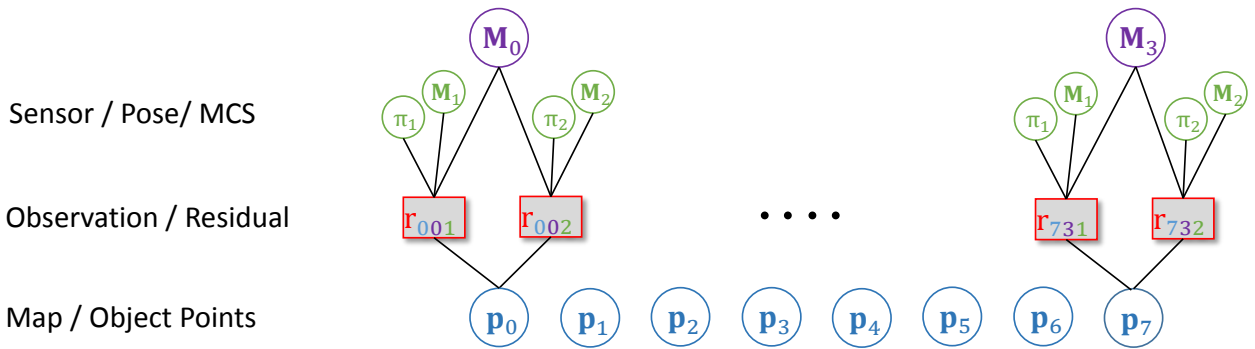


Figure 4. Depicted is the hyper graph model of MultiCol. Parameters are denoted as circles (vertices) and measurements as boxes (edges). In such a hyper graph edges can be connected to multiple vertices. In this example the $i = 1, \dots, 7$ map points p_i are observed by a MCS at a particular time from pose M_t , with $t = 1..3$. The MCS consists of $c=1..2$ cameras that have a relative orientation M_c w.r.t the body frame and an interior orientation π_c .

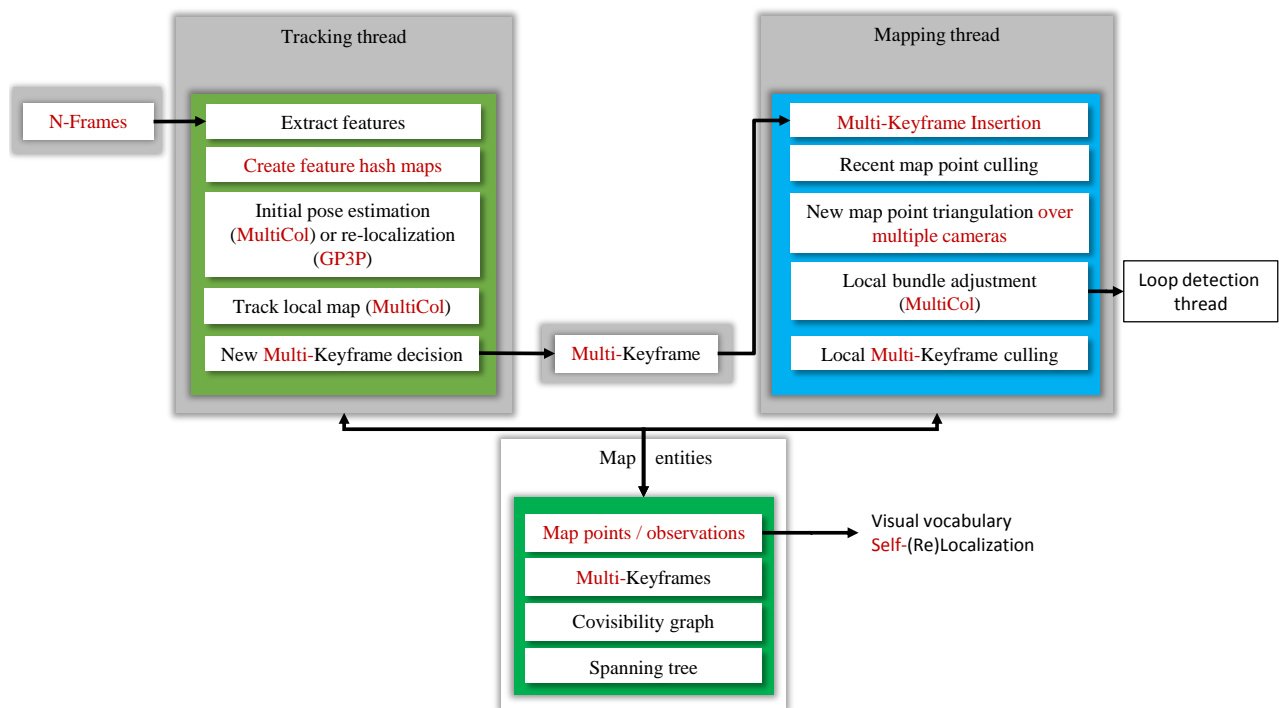


Figure 5. Depicts the MultiCol-SLAM framework without the loop closing thread. Red text depicts the modules where significant difference between our method and ORB-SLAM exist.

As FAST corners usually need a re-training in new environments, we chose to utilize AGAST (Mair et al., 2010) corners instead. Note that, in theory, none of the efficient corner extractors is suited for highly distorted (fisheye) images. To achieve a higher repeatability, the pixel positions of the Bresenham circles used for intensity testing would have to be interpolated, hence completely destroying the efficiency. Some detectors for omnidirectional images were presented in (Hansen et al., 2008, Lourenço et al., 2012). These methods report high repeatability scores, however, are too slow for real-time applications. An interesting adaptation of FAST and ORB to spherical images was proposed in (Zhao et al., 2015) called SPHORB, however, without providing the corresponding source code.

In MultiCol-SLAM, we extract ORB descriptors on each AGAST feature that is extracted in different cells over multiple scale levels keeping in mind that neither the detector nor the descriptor is particularly suited for distorted images. It shows, however, that the robust tracking and mapping back-end as well as the restriction of feature matching to local image areas (guided search) is able to compensate for the drawbacks and weaknesses of the feature extraction stage.

In addition, we extend the feature extraction module of the implementation to work with detectors and descriptors that are part of OpenCV.

Tracking from the Previous Pose This step is similar to ORB-SLAM. First, the current pose is estimated by using a constant velocity motion model. Then, local map points assigned to the last pose are projected to each camera of the current MCS and a guided search is performed around the projected location. With this initial set of matches, the MCS pose is optimized using MultiCol on fixed map points and outlier measurements are marked by identifying edges with residuals over e . With the optimized pose, the guided search is repeated, to identify more potential matches and the pose is optimized again.

Re-Localization As soon as the tracking thread indicates a tracking failure, re-localization is carried out. This happens if not enough points are retained after the initial pose tracking. Then, the images are converted into their corresponding Bag-of-Words representation, and the recognition database is queried for potential MKF candidates. We iterate through each MKF and match all associated map points to the keypoints detected in the current frame yielding a set of putative correspondences. In ORB-SLAM, the initial pose estimate is found using EPnP in a RANSAC loop.

We exchange EPnP for two reasons. On the one hand, EPnP requires more than three points to estimate the current pose of the camera and is thus not a minimal solution. The EPnP estimate is furthermore rather unstable for only few points (Urban et al., 2016a). On the other hand, as we build our system on a MCS, we try to solve for the six degrees of freedom of the MCS pose using observations from multiple cameras. Thus, GP3P+RANSAC (Kneip et al., 2013) is used to find a putative set of inliers for all MKF candidates. If enough inliers are retained and RANSAC did not exceed a predefined number of iterations, we refine the initial pose estimate obtained by GP3P for each MKF over all inliers using UPnP (Kneip et al., 2013). Finally, the pose is optimized with MultiCol, again suppressing map point correspondences with high residuals. If more than a predefined number of points (we set this to 15) is retained after final pose optimization, re-localization was successful and the tracking thread goes back into its usual behaviour.

Tracking the Local Map The final step of the tracking loop is important, as it reinforces the visual connectivity and builds a densely connected co-visibility graph. Having estimated an initial pose either from tracking the previous pose or after re-localization, the local map is projected to the MCS to find more matches. To identify which map points are contained in the local map, a reference MKF to the current pose has to be found first. Thus, we take the list of map points that are currently assigned to the MCS pose entity and from which the current pose was estimated. As each map point stores a list of MKFs it has been observed in, we can then iterate through all map points and count their occurrences. Care has to be taken, as each map point can be observed multiple times from each MKF. The MKF with the most occurrences is taken as the reference MKF and a set of local MKFs is queried from the co-visibility graph.

Then, the following steps are performed consecutively over each point \mathbf{p}_i in the local map:

- (1) Project \mathbf{p}_i into each camera of the MKF. Discard if projection is not inside the mirror boundary of a specific camera. Otherwise add the point to potential candidates.
- (2) Compute the angle between the current bearing vector \mathbf{v}_i and the map point viewing direction \mathbf{n}_i and discard if angle is larger than 50° .
- (3) Compute the distance d_i from the current MCS pose to the map point. If this distance is outside the interval d_{min} and d_{max} that are defined by the scale invariance region of the image pyramid, discard the point.
- (4) Get all descriptors around the projected location of the map point at a given scale and match them to the map point descriptor.

Finally, the pose is optimized for the last time. If not enough matches are retained, the tracking thread goes into re-localization mode.

New Multi-Keyframe Decision From a robustly estimated MKF pose that is tightly connected to the local map and co-visible MKFs the tracking thread decides if it is time to add a new MKF to the map. The insertion takes place if the following conditions are met. All thresholds are set according to the FPS of the camera system (our MCS runs at FPS = 25):

- (1) More than $0.5 \cdot \text{FPS}$ frames have passed from last MKF insertion and the local mapping thread is idle.
- (2) A certain amount of poses must be successfully tracked from the last re-localization. In our case this threshold is set to the current frame rate.
- (3) At least 50 points are tracked from the current MCS pose.
- (4) Less than 90% of the current map points are assigned to the reference MKF. Thus, MKFs are only inserted if the visual change is big enough.

4.4 Mapping Thread

This section details the mapping thread (cf. Figure 5). Asynchronously to the tracking thread, it extends the map by triangulating new points, performs local bundle adjustment and deletes redundant map points and MKFs from the map. Every time it finishes one loop, the entities are fed back to the tracking thread and become available.

Multi-Keyframe Insertion As soon as the tracking thread decides to insert a new MKF into the map, the mapping thread starts to update the co-visibility graph. The last step in the tracking thread ensured a tight connectivity. Thus a new node is added to the graph and the edge weights are updated with the number of map points each MKF shares with the new MKF. In addition, a Bag-of-Words representation of the new MKF is computed and saved in the recognition database.

Recent Map Point Deletion The mapping threads stores a list of recently added map points from the last three MKFs. All map points under consideration have to pass the following conditions to remain in the map. The conditions do not only take visibility in subsequent MKFs into account but also the appearance between them.

- (1) A map point has to be found in at least 25% of its predicted MCS poses.
- (2) The map point must be observed from at least three MKFs.

As in ORB-SLAM, a map point can only be removed from the map if it is visible in less than three MKFs. This can happen if MKFs are removed from the map.

New Map Point Triangulation over Multiple Cameras Map points are created by triangulation from MKFs. First the co-visibility graph is queried for five MKFs from the current reference MKF. Then the following iteration is carried out to create new map points:

- (1) Check if the baseline between the reference and the current neighboring MKF is big enough.
- (2) Search image points for triangulation. First the Essential matrix \mathbf{E} is calculated for each camera pair. E.g. in this case of three cameras, we get nine essential matrices in two MKFs. Those will be used to verify that matched points lie on the corresponding epipolar great circle.
- (3) Take all descriptors from the reference MKF and match them to all descriptors from the queried MKF.
- (4) Discard, if point is too far from epipolar great circle or Hamming distance is above threshold.

Finally map points are triangulated and tested for positive depth, parallax and reprojection error in both cameras from which they were triangulated. If the newly created map point passes all tests, it is added to the map, a descriptor mask is learned and it is passed to the recently added map point list, that in turn is used to cull bad map points.

Map point fusion As the triangulation step might have yielded redundant points that were already in the map, the next step is to fuse those point duplications. Therefore, the map points connected to the current MKF are first projected to all MKFs that are connected in the co-visibility graph. Within each MKF the map points are projected to each camera. Then, all features in a local area around the projected point are queried and matched. If a match is found, that also lies on the epipolar great circle, the map points are fused. If the matched image point is not connected to a map point yet, it is added as an observation. After projecting from the current to all connected MKFs, the same procedure is carried out vice versa.

Local Bundle Adjustment The local bundle adjustment optimizes over poses and map points in the inner window (cf. Figure 2). Therefore, we query the co-visibility graph from the current reference MKF to get a set of MKFs. Then, all map points that are seen from this set of MKFs are added to the local map. In addition, the outer window is found, by looping over the current set of local map points and identifying MKFs that are not yet part of the local set of MKFs. This stabilizes the trajectory and connects it to the rest of the map.

Again the MultiCol equations are used, but this time we optimize over the local map points \mathbf{p}_i and poses \mathbf{M}_t . Although hundreds of points and dozens of poses are subject to optimization, the bundle adjustment problem can be efficiently solved by exploiting the special sparsity structure of the Jacobian and Hessian respectively. The special structure comes from the fact that only point-pose but no point-point or pose-pose constraints exist. The resulting normal equations can be efficiently solved using the Schur complement trick. For more details and insights on the subject, the reader is referred to (Engels et al., 2006). Subsequently, the local map is updated and passed back to the tracking thread.

Local Multi-Keyframe Culling Like in ORB-SLAM, we delete a MKF from the map if any pair of MKFs shares more than 90% of the same map points. Instead of counting map point observations for each camera of the MCS, we count only the occurrence per MKF.

4.5 Loop Detection and Closing Thread

In this section, the loop detection and correction procedures are detailed. They are similar to the methodology proposed in (Murtal and Tardos, 2014) but extended and adapted to multi-fisheye camera systems. As measurement errors accumulate over time, the estimated trajectory starts to drift in seven degrees of freedom, i.e. translation, rotation and scale. This effect is visualized in a toy example in Figure 6. Although the MCS visits the same place, the current local map (depicted in blue) does not coincide with the historic map (depicted in gray and orange). Although the map does not spatially align with the start of the trajectory, its local map structure is very similar assuming that the system reconstructs a large amount of map points at the same location, i.e. the reconstruction is repeatable. The goal of the loop detection thread is to identify the situation depicted in Figure 6. It detects the loop candidates from the historic trajectory and corrects the loop by propagating the loop closing error along the trajectory.

The loop detection and correction procedure, as well as the place recognition database and visual vocabulary components are depicted in Figure 7. Each step is detailed in the following sections.

Candidate detection As soon as the system revisits a place or parts of a scene it has seen and reconstructed before, it should load the associated local map points and start tracking from them instead of starting to reconstruct the scene again. This, however, is a challenging task, as the local map is solely queried from the co-visibility graph. One possible way would be to query the map points spatially, i.e. that we query the nearest neighbor map points in a specified radius from the current MKF. This method could work for smaller loops, but as soon as larger loops occur, the corresponding local maps could lie dozens of meters apart, which is sketched in Figure 6. A more favorable solution is to use visual cues to identify possible loop candidates.

After local bundle adjustment, the current multi-keyframe MKF_i is handed over to the loop detection and correction thread. Now the MKF database could be directly queried for visually similar MKFs. However, the number of database results has to be limited

somehow. This could either be achieved by taking a fixed number of MKFs sorted by their similarity score. Latter, however, is an absolute measure whose magnitude is unknown, e.g. we queried 10 MKFs, but all have a very bad similarity score. Thus a way of getting a relative measure of the quality of the current similarity score is needed.

Hence, the BoW vectors of all MKFs that are connected in the co-visibility graph of the current MKF_{*i*} are queried. Then, the similarity score between all BoW vectors and the current MKF BoW vector are calculated. The lowest score s_{sim} is taken as a similarity threshold, i.e. we only take MKFs from the database as candidates if their score is higher than s_{sim} and thus more similar, than the most dissimilar MKF in the co-visibility graph.

To further reduce the number of possible false candidates, MKF candidates are only accepted if they are part of a consistent group of connected MKFs in the co-visibility graph after several consecutive MKF insertions. Each loop candidate is connected to a number of MKFs (a group) in the co-visibility graph. A group is accepted to be consistent with the previous group if it they share a MKF.

Transformation estimation If one or more candidates are accepted, the similarity transformation between the current MKF_{*i*} and all candidates can be estimated. Lets assume for now, that we have one candidate MKF_{*c*}. Looking back at Figure 6, the goal is to find the similarity transformation \mathbf{S} between the map points \mathbf{p}^i assigned to MKF_{*i*} and the map points \mathbf{p}^c assigned to MKF_{*c*}:

$$\mathbf{p}_{mcs}^i = \mathbf{S}\mathbf{p}_{mkf}^c = \begin{bmatrix} s\mathbf{R} & \mathbf{T} \\ \mathbf{0}^T & 1 \end{bmatrix} \mathbf{p}_{mkf}^c \quad (2)$$

Instead of taking all map points that are connected to both frames, the descriptors assigned to each map point by the MKF are matched in advance. This leaves us with a subset of possible map point correspondences. Yet, this set contains outliers that are either caused by wrong descriptor matches or the distance ratios between reconstructed points is too big, caused by bad reconstruction. Hence, RANSAC is used to find a similarity transformation using Horn’s quaternion ((Horn et al., 1988)) method as a model and thus 3D-3D¹ correspondences.

First the set of map points matches is transformed to the respective MKF:

$$\mathbf{p}_{mkf}^c = \mathbf{M}_t^c \mathbf{p}^c \quad \mathbf{p}_{mkf}^i = \mathbf{M}_t^i \mathbf{p}^i \quad (3)$$

where \mathbf{M}_t is the respective pose of the MKF. Obviously, the points can not be transformed to each camera of the MKF, as map points can be observed from multiple cameras and the only common frame is the MKF frame.

Subsequently RANSAC iterations are performed. Three points are selected from each point cloud, and the transformation is estimated. To decide whether the transformation is accepted, the map points are transformed from MKF_{*c*} to MKF_{*i*} and vice versa using the estimated similarity:

$$\hat{\mathbf{p}}_{mkf}^i = \mathbf{S}\mathbf{p}_{mkf}^c \quad \hat{\mathbf{p}}_{mkf}^c = \mathbf{S}^{-1}\mathbf{p}_{mkf}^i \quad (4)$$

¹Recently, new methods were proposed, that solve the generalized relative orientation and scale problem (similarity between MCSs) using 2D-3D (Sweeney et al., 2014) or 2D-2D (Sweeney et al., 2015a) correspondences only to compute \mathbf{S} . Latter would alleviate the effects of reconstruction error, however, depends on an additional constraint, i.e. the current vertical direction needs to be determined. We leave the integration and investigation to future work.

Subsequently the points are transformed to the camera frames and projected to the image plane. Now, the reprojection error can be computed and used to determine the number of inliers. If the transformation yields enough inliers, a guided matching is instantiated to search for more correspondences, also between cameras. Then, \mathbf{S} is optimized by minimizing the reprojection errors of both transformed point sets (Equation 4) in both MKFs. The optimization is again carried out using g2o and outliers are down-weighted using a Huber kernel. If more than 20 inliers are retained after optimization, \mathbf{S} is accepted and the loop correction is started.

Loop correction and fusion The first step to loop correction is, to correct all MKFs that are connected to the current MKF_{*i*}, as well as all map points that are part of the local map. After this step, the local maps spanned by MKF_{*i*} and MKF_{*c*} should align. The corrected pose $\hat{\mathbf{M}}_t$ of a MKF is computed by first estimating the relative orientation between pose \mathbf{M}_t^i of the current MKF_{*i*} and the MKF pose \mathbf{M}_t and subsequent correction using the similarity:

$$\hat{\mathbf{M}}_t = (\mathbf{M}_t \mathbf{M}_t^i)^{-1} \mathbf{S} \quad (5)$$

Subsequently, the map points need to be corrected as well. First, each map point is rotated to the MKF frame using the uncorrected pose. Then, the point is transformed to the corrected map point position $\hat{\mathbf{p}}$ by applying the inverse of the corrected MKF pose, i.e. the map point is directly transformed back into world coordinates:

$$\hat{\mathbf{p}} = \hat{\mathbf{M}}_t^{-1} (\mathbf{M}_t \mathbf{p}) \quad (6)$$

The correction of the local map will result in many point duplications and redundant MKFs. Thus the same map point fusion procedure presented in Section 4.4 is carried out and the co-visibility graph is updates.

Finally, the essential graph is optimized. First, all MKF poses \mathbf{M}_t are converted to similarities \mathbf{S}_t by initially setting the scale to 1.0. Then, the relative pose constrains between all MKFs in the map are computed:

$$\Delta \mathbf{M}_{ij} = \mathbf{M}_j \mathbf{M}_i^{-1} \quad (7)$$

between some MKF i and j . Again, all relative pose constrains are converted to similarities $\Delta \mathbf{S}_{ij}$. The optimization is carried out over pose-pose constrains and follows the work of (Strasdat et al., 2010). The residual that we try to minimize is defined as:

$$\mathbf{r}_{i,j} = \log_{Sim(3)}(\Delta \mathbf{S}_{ij} \mathbf{S}_i \mathbf{S}_j^{-1}) \quad (8)$$

where the log is the inverse relation of the exponential map (see (Strasdat, 2012)). The goal of the optimization is to adjust \mathbf{S}_i and \mathbf{S}_j such that the transformation sequence (back and forth between both MKFs) is as close to the identity as possible. In the beginning, all residual transformations Equation 8 will be the identity except for the part of the map, that was corrected above. Then the error is propagated back over all pose-pose constrains during optimization as the similarities \mathbf{S}_i and \mathbf{S}_j are gradually changed to optimally fit the loop closure constrain.

We optimize only the transformations between MKFs that are connected by at least 100 points, i.e. that the edge weight in the co-visibility graph is above 100. After optimization, all map points are corrected:

$$\hat{\mathbf{p}} = \hat{\mathbf{S}}_t^{-1} (\mathbf{M}_t \mathbf{p}) \quad (9)$$

using the corrected MKF pose $\hat{\mathbf{S}}_t$. and finally all $\hat{\mathbf{S}}_t$ are converted

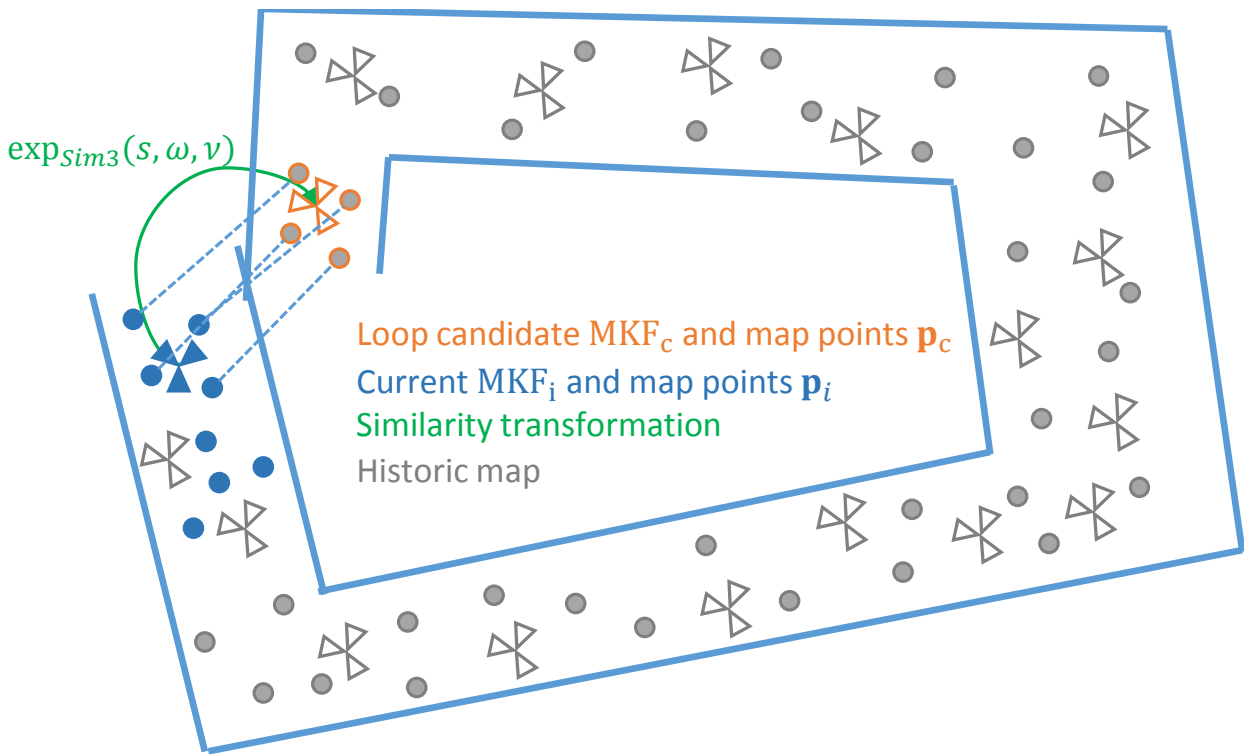


Figure 6. Depicts the loop closing problem. If the SLAM trajectory was estimated without drift, the orange and blue map points should coincide. As this is in general not the case, a similarity transformation can be estimated that aligns both parts of the trajectory over the map points. Then, the alignment error can be used to correct the remaining MKF poses and map points by projecting it back through the map.

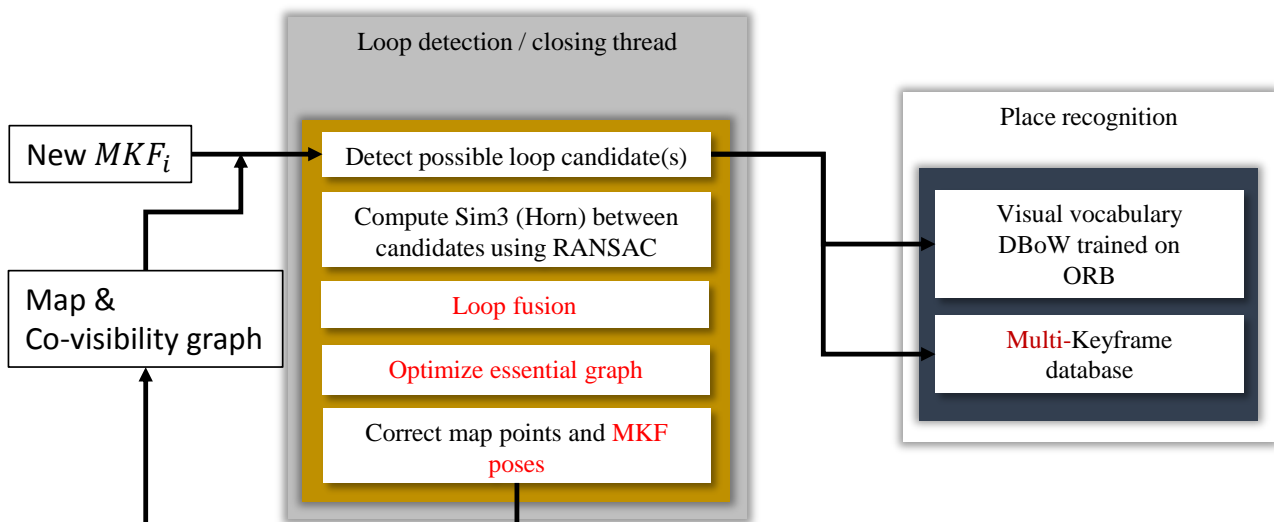


Figure 7. Depicts the loop detection and correction thread. It extends Figure 5. Each time a new MKF is inserted, the loop detection thread tries to detect possible loop candidates from the MKF database. First, a BoW score s_{min} is computed for all frames that are connected to the new MKF in the co-visibility graph. Then the MKF database is queried and only MKFs with a score higher than s_{min} are declared as candidates for loop detection. The right part shows the two components of the place recognition class.

back to rigid body transformations:

$$\mathbf{M}_t = \begin{bmatrix} \mathbf{R} & \mathbf{t}/s \\ \mathbf{0}^T & 0 \end{bmatrix} \quad (10)$$

where s is the scale.

5. EXPERIMENTS AND RESULTS

To test the performance of the presented MCS SLAM, various tests are performed. More information about the dataset can be found on (Urban and Jutzi, 2016). First, we evaluate the impact of using multiple fisheye cameras instead of one, in terms of accuracy, runtime, successfully tracked frames and loop closing.

To evaluate the accuracy of SLAM systems, two metrics are commonly used that compare the estimated camera poses \mathbf{M}_t to a ground truth pose \mathbf{M}_t^{gt} at some time t or an interval Δt . The difference between these two poses at time t is given by the relative orientation between them:

$$\mathbf{M}_t^{rel} = \mathbf{M}_t^{gt-1} \mathbf{M}_t \quad (11)$$

The first metric is called ATE and estimates the root mean squared translation differences between both trajectories. In order to calculate the absolute error, the two trajectories need to be aligned in advance using a similarity transformation \mathbf{S} . For N pose pairs, the ATE can then be calculated as:

$$\text{ATE} = \sqrt{\frac{1}{N} \sum_{t=1}^N \|\text{trans}(\mathbf{M}_t^{rel})\|^2} \quad (12)$$

$$= \sqrt{\frac{1}{N} \sum_{t=1}^N \|\text{trans}(\mathbf{M}_t^{gt-1} \mathbf{S} \mathbf{M}_t)\|^2} \quad (13)$$

where "trans" returns the translational component of the transformation matrix \mathbf{M} .

The second metric is called RPE and allows to evaluate the local accuracy and drift of the trajectory over some time interval Δ . Thus we can calculate $M = N - \Delta$ relative orientation errors along the trajectory. The RPE at time step t can be defined by:

$$\text{RPE}(\Delta) = \sqrt{\frac{1}{M} \sum_{t=1}^M \|\text{trans}(\mathbf{M}_t^{rel})\|^2} \quad (14)$$

but this time the relative transformation is defined as:

$$\mathbf{M}_t^{rel} = (\mathbf{M}_t^{gt-1} \mathbf{M}_{t+\Delta}^{gt})^{-1} (\mathbf{M}_t^{-1} \mathbf{M}_{t+\Delta}) \quad (15)$$

To calculate the relative error of subsequent poses we set $\Delta = 1$. In the case of ATE only the translation is evaluated. For the relative error, we can also evaluate the rotational accuracy. This is done by replacing the "trans" with a function that returns the Rodriguez vector of the rotation matrix in \mathbf{M} .

Each trajectory is evaluated five times, i.e. the SLAM algorithms are used five times to estimate the camera trajectory. All accuracies and run-times are calculated as the median value over the five runs.

5.1 Single- vs. Multi-Camera SLAM

First, we align the KFs or MKFs respectively, by estimating a similarity transformation between ground truth and SLAM trajectory. Then, the ATE (Equation 13) is evaluated for all trajectories. The results are depicted in Table 9a. Obviously, MultiCol-SLAM significantly outperforms its single camera pendant in terms of Keyframe accuracy. One explanation of the large performance gap is the simple initialization of the single camera SLAM. The

authors of ORB-SLAM proposed an initialization based on homography and fundamental matrix estimation. Both matrices can not be readily computed for the camera model employed in this work. Thus we simply initialize the single camera SLAM by estimating the essential matrix and selecting a solution based on a threshold on the magnitude of the translation vector, which is obviously less robust than the method proposed in (Mur-Artal and Tardos, 2014).

To get a measure of the local accuracy, we also estimate the RPE (Equation 14) for all trajectories and all poses by setting $\Delta = 1$. The trajectories do not need to be aligned in this case. The accuracies for translation and rotation are depicted in Table 9b. Still, using multi-cameras yields a better performance, especially for the translation. The rotational components show a similar trend, but the differences are less prominent. The rotational accuracy for the two lasertracker trajectories is a lot better because the trajectory has only little rotation of the camera system about the up-axis. On average the rotational accuracy of the MCS is about 0.5-1.5° and the translational component, depending on the walking speed and scene between 1.0-2.5 cm.

6. SUMMARY AND CONCLUSION

In this paper MultiCol-SLAM, a real-time multi-fisheye camera SLAM system was proposed. First, we recapitulated the current state-of-the-art in the field and argued why keyframe-based approaches outperform filter-based SLAM systems. Then we subsumed the MultiCol model and detailed our contributions. Subsequently, we elaborately detailed our framework that builds upon ORB-SLAM and is divided into several threads running in parallel. Finally, all proposed modules were examined using accurate ground-truth data and it showed, that using multi-camera systems helps to improve the accuracy and robustness of SLAM in challenging environments.

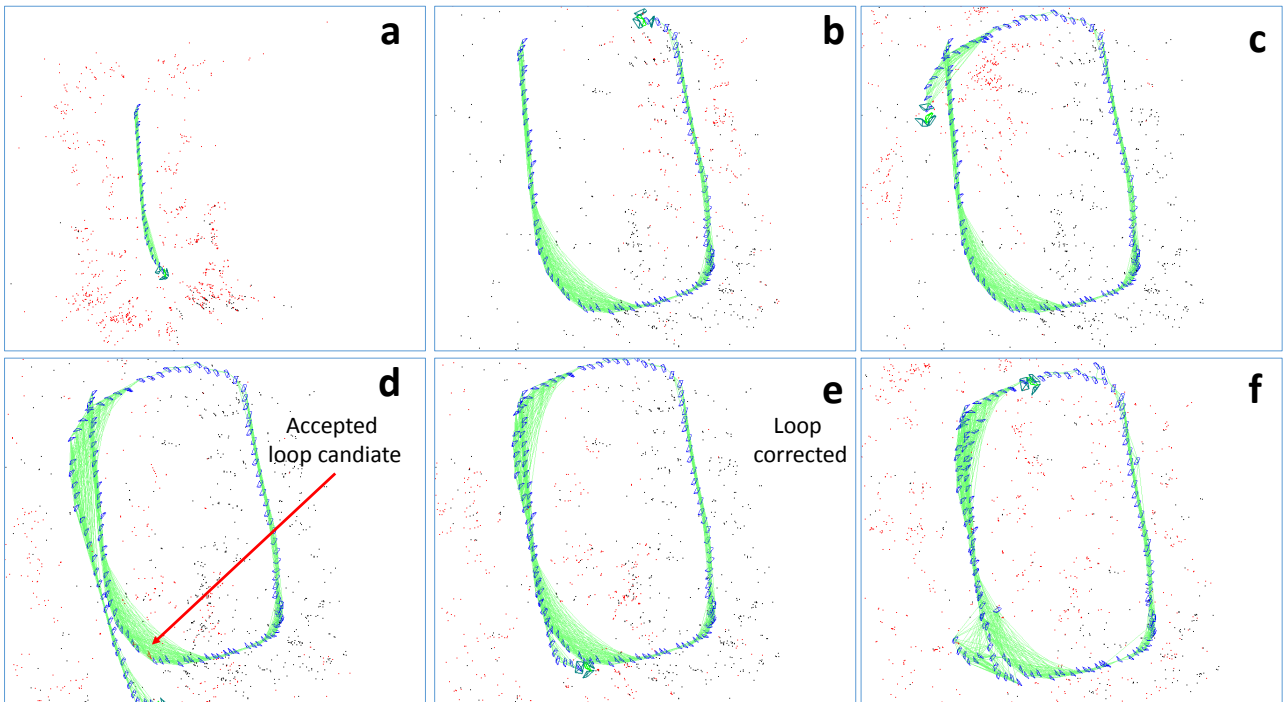
In addition, we make the proposed SLAM system available to the public (<https://github.com/urbste/MultiCol-SLAM>) and hope that it helps to further encourage research in multi-camera egomotion estimation and related topics.

ACKNOWLEDGMENT

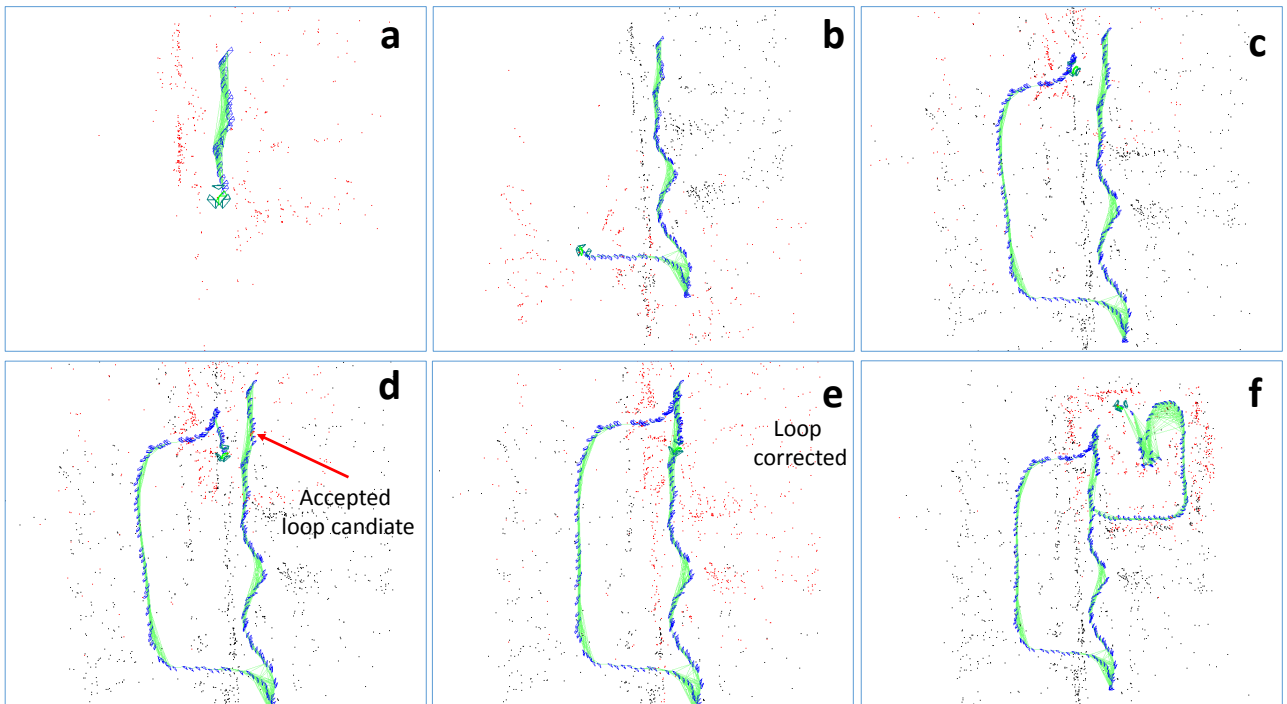
This project was partially funded by the DFG research group FG 1546 "Computer-Aided Collaborative Subway Track Planning in Multi-Scale 3D City and Building Models".

REFERENCES

- Agarwal, S., Snavely, N., Simon, I., Seitz, S. M. and Szeliski, R., 2009. Building rome in a day. In: Proceedings of the International Conference on Computer Vision (ICCV), IEEE, pp. 72–79.
- Barreto, J. P. and Daniilidis, K., 2005. Fundamental Matrix for Cameras With Radial Distortion. In: Proceedings of the International Conference on Computer Vision (ICCV), Vol. 1, IEEE, pp. 625–632.
- Cadena, C., Carlone, L., Carrillo, H., Latif, Y., Scaramuzza, D., Neira, J., Reid, I. D. and Leonard, J. J., 2016. Simultaneous Localization And Mapping: Present, Future, and the Robust-Perception Age. CoRR.
- Caruso, D., Engel, J. and Cremers, D., 2015. Large-Scale Direct SLAM for Omnidirectional Cameras. In: Proceedings of the IEEE/RSJ Conference on Intelligent Robots and Systems (IROS).
- Concha, A. and Civera, J., 2015. DPPTAM: Dense Piecewise Planar Tracking and Mapping from a Monocular Sequence. In: Proceedings of the IEEE/RSJ Conference on Intelligent Robots and Systems (IROS), IEEE, pp. 5686–5693.



(a) Trajectory 1



(b) Trajectory 2

Figure 8. Depicted are two successful loop closures. **a-b** trajectory and map is build. The green lines represent the co-visibility graph edges with a weight higher than 100. Blue pyramids depict MKF. Red map points is the active map, black points are all map points. **c** Visually the trajectory crossed itself. However no loop is detected. Although candidates exist, RANSAC does not find a good solution, because the reconstructed geometry is still too different. **d** a loop candidate is accepted. **e** The corrected loop after the optimization of the essential graph. **f** tracking continues using the active map. New MKFs are only created if the baseline is large enough or to few points are tracked.

	Single fisheye camera	Multi-fisheye camera system	Single fisheye camera	Multi-fisheye camera system
	[cm]	[cm]	[cm]/[deg]	[cm]/[deg]
Laser 1	31.0	1.4	1.95/0.32	1.2/0.33
Laser 2 fast	28.1	5.3	2.6/0.31	2.7/0.56
Indoor 1 stat. env.	32.4	2.1	2.8/1.72	1.1/1.54
Indoor 2 dyn. env.	13.3	1.8	2.8/2.04	1.1/1.78
Outdoor 1 dyn. env	(X)	3.6	(X)	2.3/1.28

(a) ATE
(b) RPE

Figure 9. (a) Median KF and MKF ATEs for single and multi-camera SLAM respectively. The translational accuracy was calculated after 7DoF alignment between ground truth and estimated frames. (b) RPE for single and multi-fisheye camera SLAM. Here we set $\Delta = 1$, i.e. the frame two frame tracking accuracy is estimated. (X) means that tracking failed at some point and a significant part of the trajectory was not tracked.

Thread	Operation	Single fisheye camera	Multi-fisheye camera system
Tracking	Frame creation	12/12/2	21/23/5
	Pose estimation	4/4/1	3/4/3
	Track local map	5/5/2	4/5/4
	Total	21	28
Mapping	Map point creation	27/26/10	96/96/17
	Map point fusion	11/11/6	11/12/9
	Local BA	185/198/125	170/174/65
	Total	223	277

Table 1. Depicted is the time (mean, median and standard deviation) for each step in different threads. In case of Single camera SLAM, we extracted 1000 features. In case of multi-camera SLAM 400 features per camera are extracted and the extraction is performed in parallel. The pose estimation is slower in the single camera case, as no analytical Jacobian was provided.

Cummins, M. and Newman, P., 2010. Invited Applications Paper FAB-MAP: Appearance-Based Place Recognition and Mapping using a Learned Visual Vocabulary Model. In: Proceedings of the International Conference on Machine Learning (ICML).

Davison, A. J., Cid, Y. G. and Kita, N., 2004. Real-Time 3D SLAM With Wide-Angle Vision. In: Proceedings of the IFAC Symposium on Intelligent Autonomous Vehicles (IAV).

Davison, A. J., Reid, I. D., Molton, N. D. and Stasse, O., 2007. MonoSLAM: Real-Time Single Camera SLAM. IEEE Transactions on Pattern Analysis and Machine Intelligence (PAMI) 29(6), pp. 1052–1067.

Dellaert, F. and Kaess, M., 2006. Square Root SAM: Simultaneous Localization and Mapping Via Square Root Information Smoothing. International Journal of Robotics Research (IJRR) 25(12), pp. 1181–1203.

Engel, J., Schöps, T. and Cremers, D., 2014. LSD-SLAM: Large-scale direct monocular SLAM. In: Proceedings of the European Conference on Computer Vision (ECCV), Springer, pp. 834–849.

Engel, J., Stücker, J. and Cremers, D., 2015. Large-scale direct slam with stereo cameras. In: Proceedings of the IEEE/RSJ Conference on Intelligent Robots and Systems (IROS).

Engels, C., Stewénius, H. and Nistér, D., 2006. Bundle Adjustment Rules. Photogrammetric computer vision 2, pp. 124–131.

Forster, C., Pizzoli, M. and Scaramuzza, D., 2014. SVO: Fast semi-direct monocular visual odometry. In: Proceedings of the IEEE International Conference on Robotics and Automation (ICRA), IEEE, pp. 15–22.

Gálvez-López, D. and Tardós, J. D., 2012. Bags of binary words for fast place recognition in image sequences. IEEE Transactions on Robotics 28(5), pp. 1188–1197.

García-Fidalgo, E. and Ortiz, A., 2015. Vision-based topological mapping and localization methods: A survey. Robotics and Autonomous Systems 64, pp. 1–20.

Gauglitz, S., Höllerer, T. and Turk, M., 2011. Evaluation of interest point detectors and feature descriptors for visual tracking. International Journal of Computer Vision (IJCV) 94(3), pp. 335–360.

Hansen, P., Boles, W. and Corke, P., 2008. Spherical Diffusion for Scale-Invariant Keypoint Detection in Wide-Angle Images. In: Proceedings of the Digital Image Computing on Techniques and Applications (DICTA), IEEE, pp. 525–532.

Harmat, A., Sharf, I. and Trentini, M., 2012. Parallel Tracking and Mapping with Multiple Cameras on an Unmanned Aerial Vehicle. In: Intelligent robotics and applications, Springer, pp. 421–432.

Harmat, A., Trentini, M. and Sharf, I., 2015. Multi-Camera Tracking and Mapping for Unmanned Aerial Vehicles in Unstructured Environments. Journal of Intelligent & Robotic Systems 78(2), pp. 291–317.

Hartley, R. I. and Zisserman, A., 2008. Multiple view geometry in computer vision. University Press, Cambridge, UK.

Heng, L., Lee, G. H. and Pollefeys, M., 2014. Self-calibration and visual slam with a multi-camera system on a micro aerial vehicle. In: Proceedings of Robotics: Science and Systems (RSS).

Horn, B. K. P., Hilden, H. M. and Negahdaripour, S., 1988. Closed-Form Solution of Absolute Orientation using Orthonormal Matrices. Journal of the Optical Society of America 5, pp. 1127–1136.

Kerl, C., Sturm, J. and Cremers, D., 2013. Dense visual SLAM for RGB-D cameras. In: Proceedings of the IEEE/RSJ Conference on Intelligent Robots and Systems (IROS), IEEE, pp. 2100–2106.

Klein, G. and Murray, D., 2007. Parallel tracking and mapping for small AR workspaces. In: Proceedings of the International Symposium on Mixed and Augmented Reality (ISMAR), IEEE, pp. 225–234.

Klein, G. and Murray, D., 2008. Improving the agility of keyframe-based SLAM. In: Proceedings of the European Conference on Computer Vision (ECCV), Springer, pp. 802–815.

Klein, G. and Murray, D., 2009. Parallel tracking and mapping on a camera phone. In: Proceedings of the International Symposium on Mixed and Augmented Reality (ISMAR), IEEE, pp. 83–86.

Kneip, L. and Li, H., 2014. Efficient Computation of Relative Pose for Multi-Camera Systems. In: Proceedings of the IEEE Conference on Computer Vision and Pattern Recognition (CVPR), pp. 446–453.

Kneip, L., Furgale, P. and Siegwart, R., 2013. Using Multi-Camera Systems in Robotics: Efficient Solutions to the NPNP Problem. In: Proceedings of the IEEE International Conference on Robotics and Automation (ICRA), IEEE, pp. 3770–3776.

- Kneip, L., Siegart, R. and Pollefeys, M., 2012. Finding the exact rotation between two images independently of the translation. Springer.
- Kraus, K., 2004. Photogrammetrie: Geometrische Informationen aus Photographien und Laserscanneraufnahmen. Walter de Gruyter.
- Kukelova, Z., Heller, J., Bujnak, M. and Pajdla, T., 2015. Radial distortion homography. In: Proceedings of the IEEE Conference on Computer Vision and Pattern Recognition (CVPR), pp. 639–647.
- Kummerle, R., Grisetti, G., Strasdat, H., Konolige, K. and Burgard, W., 2011. G^2o : A General Framework for Graph Optimization. In: Proceedings of the IEEE International Conference on Robotics and Automation (ICRA), IEEE, pp. 3607–3613.
- Lepetit, V., Moreno-Noguer, F. and Fua, P., 2009. EPnP: An Accurate O(n) Solution to the PnP Problem. International Journal of Computer Vision (IJCV) 81(2), pp. 155–166.
- Lim, H., Lim, J. and Kim, H. J., 2014. Real-Time 6-DoF Monocular Visual SLAM in a Large-Scale Environment. In: Proceedings of the IEEE International Conference on Robotics and Automation (ICRA), IEEE, pp. 1532–1539.
- Lin, K.-H., Chang, C.-H., Dopfer, A. and Wang, C.-C., 2012. Mapping and Localization in 3D Environments Using a 2D Laser Scanner and a Stereo Camera. Journal of information science and engineering 28(1), pp. 131–144.
- Lourenço, M., Barreto, J. P. and Vasconcelos, F., 2012. sRD-SIFT: Keypoint Detection and Matching in Images with Radial Distortion. IEEE Transactions on Robotics 28(3), pp. 752–760.
- Luhmann, T., Robson, S., Kyle, S. and Harley, I., 2006. Close Range Photogrammetry: Principles, Methods and Applications. Whittles.
- Mair, E., Hager, G. D., Burschka, D., Suppa, M. and Hirzinger, G., 2010. Adaptive and Generic Corner Detection Based on the Accelerated Segment Test. In: Proceedings of the European Conference on Computer Vision (ECCV).
- Montemerlo, M. and Thrun, S., 2007. FastSLAM 2.0. FastSLAM: A Scalable Method for the Simultaneous Localization and Mapping Problem in Robotics pp. 63–90.
- Montemerlo, M., Thrun, S., Koller, D., Wegbreit, B. et al., 2002. FastSLAM: A Factored Solution to the Simultaneous Localization and Mapping Problem. In: AAAI/IAAI, pp. 593–598.
- Mur-Artal, R. and Tardos, J. D., 2014. ORB-SLAM: tracking and mapping recognizable features. In: Proceedings of Robotics: Science and Systems (RSS).
- Mur-Artal, R. and Tardós, J. D., 2015. Probabilistic Semi-Dense Mapping from Highly Accurate Feature-Based Monocular SLAM. Proceedings of Robotics: Science and Systems, Rome, Italy.
- Mur-Artal, R. and Tardos, J. D., 2016. ORB-SLAM2: an Open-Source SLAM System for Monocular, Stereo and RGB-D Cameras. ArXiv e-prints.
- Mur-Artal, R., Montiel, J. M. M. and Tardós, J. D., 2015. ORB-SLAM: a Versatile and Accurate Monocular SLAM System. IEEE Transactions on Robotics 31(5), pp. 1147–1163.
- Newcombe, R. A., Lovegrove, S. J. and Davison, A. J., 2011. DTAM: Dense tracking and mapping in real-time. In: Proceedings of the International Conference on Computer Vision (ICCV), IEEE, pp. 2320–2327.
- Pirker, K., Rüther, M. and Bischof, H., 2010. Histogram of Oriented Cameras-A New Descriptor for Visual SLAM in Dynamic Environments. In: Proceedings of the British Machine Vision Conference (BMVC), pp. 1–12.
- Pirker, K., Rüther, M. and Bischof, H., 2011. CD SLAM-Continuous Localization and Mapping in a Dynamic World. In: Proceedings of the IEEE/RSJ Conference on Intelligent Robots and Systems (IROS), IEEE, pp. 3990–3997.
- Scaramuzza, D., Martinelli, A. and Siegart, R., 2006. A Toolbox for Easily Calibrating Omnidirectional Cameras. In: Proceedings of the Annual Conference of the Robotics Society of Japan (RSJ), IEEE, pp. 5695–5701.
- Schöps, Thomas, T., Engel, J. and Cremers, D., 2014. Semi-Dense Visual Odometry for AR on a Smartphone. In: Proceedings of the International Symposium on Mixed and Augmented Reality (ISMAR), IEEE, pp. 145–150.
- Snavely, N., Seitz, S. M. and Szeliski, R., 2006. Photo Tourism: Exploring Photo Collections in 3D. In: ACM transactions on graphics (TOG), Vol. 25, pp. 835–846.
- Stewenius, H., Engels, C. and Nistér, D., 2006. Recent Developments on Direct Relative Orientation. ISPRS Journal of Photogrammetry and Remote Sensing 60(4), pp. 284–294.
- Stewenius, H., Nistér, D., Oskarsson, M. and Åström, K., 2005. Solutions to Minimal Generalized Relative Pose Problems. In: Workshop on Omnidirectional Vision, Vol. 1 number 2, p. 3.
- Strasdat, H., 2012. Local Accuracy and Global Consistency for Efficient Visual Slam. PhD thesis, Citeseer.
- Strasdat, H., Davison, A. J., Montiel, J. and Konolig, K., 2011. Double Window Optimisation for Constant Time Visual SLAM. In: Proceedings of the International Conference on Computer Vision (ICCV), IEEE, pp. 2352–2359.
- Strasdat, H., Montiel, J. and Davison, A. J., 2010. Scale Drift-Aware Large Scale Monocular SLAM. In: Robotics: Science and Systems, Vol. 2, p. 5.
- Strasdat, H., Montiel, J. M. and Davison, A. J., 2012. Visual SLAM: Why Filter? Image and Vision Computing 30, pp. 65–77.
- Sweeney, C., Fragoso, V., Höllerer, T. and Turk, M., 2014. gDLS: A Scalable Solution to the Generalized Pose and Scale Problem. In: Proceedings of the European Conference on Computer Vision (ECCV), Springer, pp. 16–31.
- Sweeney, C., Kneip, L., Hollerer, T. and Turk, M., 2015a. Computing Similarity Transformations from Only Image Correspondences. In: Proceedings of the IEEE Conference on Computer Vision and Pattern Recognition, pp. 3305–3313.
- Sweeney, C., Sattler, T., Hollerer, T., Turk, M. and Pollefeys, M., 2015b. Optimizing the Viewing Graph for Structure-from-Motion. In: Proceedings of the International Conference on Computer Vision (ICCV), pp. 801–809.
- Szeliski, R., 2010. Computer Vision: Algorithms and Applications. Springer Science & Business Media.
- Triggs, B., McLauchlan, P. F., Hartley, R. I. and Fitzgibbon, A. W., 2000. Bundle Adjustment-a Modern Synthesis. In: Vision algorithms: theory and practice, Springer, pp. 298–372.
- Urban, S. and Jutzi, B., 2016. LaFiDa - A Laserscanner Multi-Fisheye Camera Dataset. Journal of Imaging.
- Urban, S., Leitloff, J. and Hinz, S., 2015. Improved Wide-Angle, Fisheye and Omnidirectional Camera Calibration. ISPRS Journal of Photogrammetry and Remote Sensing 108, pp. 72–79.
- Urban, S., Leitloff, J. and Hinz, S., 2016a. MLPnP: A Real-Time Maximum Likelihood Solution to the Perspective-N-Point problem. ISPRS Annals of the Photogrammetry, Remote Sensing and Spatial Information Science.
- Urban, S., Wursthorn, S., Leitloff, J. and Hinz, S., 2016b. Multi-Col Bundle Adjustment: A Generic Method for Pose Estimation, Simultaneous Self-Calibration and Reconstruction for Arbitrary Multi-Camera Systems. International Journal of Computer Vision (IJCV) pp. 1–19.
- Ventura, J., Arth, C. and Lepetit, V., 2015. An Efficient Minimal Solution for Multi-Camera Motion. In: Proceedings of the International Conference on Computer Vision (ICCV), pp. 747–755.
- Weinmann, M., 2013. Visual Features - From Early Concepts to Modern Computer Vision. In: Advanced Topics in Computer Vision, Springer, pp. 1–34.
- Wu, C., 2013. Towards Linear-Time Incremental Structure from Motion. In: 2013 International Conference on 3D Vision-3DV, IEEE, pp. 127–134.
- Wu, C., Agarwal, S., Curless, B. and Seitz, S. M., 2011. Multicore Bundle Adjustment. In: Proceedings of the IEEE Conference on Computer Vision and Pattern Recognition (CVPR), IEEE, pp. 3057–3064.

Yu, J. and McMillan, L., 2004. General Linear Cameras. In: Proceedings of the European Conference on Computer Vision (ECCV), Springer, pp. 14–27.

Zhao, Q., Feng, W., Wan, L. and Zhang, J., 2015. SPHORB: A Fast and Robust Binary Feature on the Sphere. International Journal of Computer Vision (IJCV) 113(2), pp. 143–159.

Zou, D. and Tan, P., 2013. COSLAM: Collaborative Visual Slam in Dynamic Environments. IEEE Transactions on Pattern Analysis and Machine Intelligence (PAMI) 35(2), pp. 354–366.